Chapter 2
Completely Packed Loop Models

2.1 Introduction

We begin with a class of three-dimensional loop models that show transitions between two types of phase—one with infinite loops, and one with only short loops. In particular, we focus on a family of completely packed models that may be viewed as discretisations of sigma models with target space CP^{n-1} (and RP^{n-1}). These loop models capture the universal behaviour of a surprising variety of classical and quantum systems—including $(2+1)$-dimensional $SU(n)$ antiferromagnets (generalising the connection for $(1+1)$D spin chains reviewed in Sect. 1.4.2), Anderson localisation in symmetry class C [1–4], line defects in random media [5], and certain models for polymers.

We will return to some of these connections in later chapters. Our aims here are to establish the continuum descriptions of the loop models, and to use these descriptions to characterise their phase transitions and the universal properties of geometrical observables. A short summary was given in Sect. 1.9.1, so we move immediately to concrete models.

2.2 Definitions

Take any four-coordinated, directed lattice on which two links enter and two links exit each node. On such a lattice we may generate a configuration of oriented loops by picking a pairing of incoming and outgoing links at each node. We assign weight p to one such pairing and weight $1-p$ to the other, so that if N_p and N_{1-p} are the numbers of nodes where the weight p and $1-p$ pairings are followed, the total weight associated with the nodes in a configuration $\mathcal{C}$ is

$$W_{\mathcal{C}} = p^{N_p}(1-p)^{N_{1-p}}. \tag{2.1}$$

A. Nahum, *Critical Phenomena in Loop Models*, Springer Theses,
DOI 10.1007/978-3-319-06407-9_2

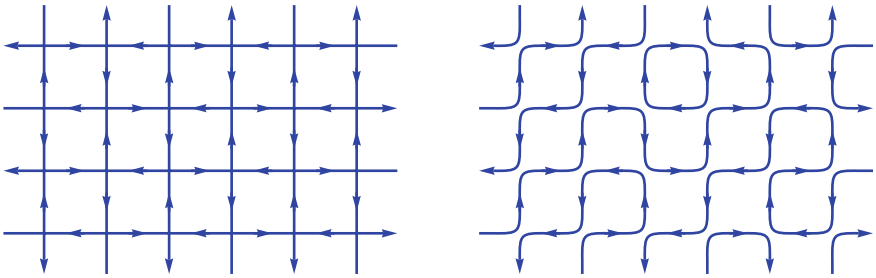

Fig. 2.1 The 2D 'L' lattice and a configuration obtained by resolving the nodes

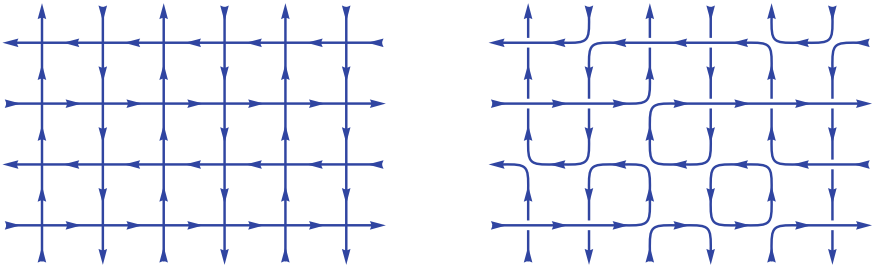

Fig. 2.2 The 2D Manhattan lattice and a configuration obtained by resolving the nodes

In addition we assign the loops a fugacity n. Denoting the number of loops by $|\mathcal{C}|$, the partition function is

$$Z_{\text{loops}} = \sum_{\mathcal{C}} n^{|\mathcal{C}|} W_{\mathcal{C}}. \tag{2.2}$$

The fugacity may also be generated by summing over n possible colours for each loop.

In the special case $n = 1$, the nodes are independent and the parameter p is simply the probability of a given node configuration. The problem is then akin to percolation: while the local degrees of freedom have trivial correlation functions, geometrical observables show nontrivial behaviour.

Various models can be constructed on the above lines, depending on the choice of lattice and the assignment of node parameters. The best-studied case is the loop model on the two-dimensional L lattice (Fig. 2.1), where weight p is associated with right-turning nodes and weight $1 - p$ with left-turning nodes (Fig. 2.3, left). This model may be mapped to the n^2-state Potts model via the Fortuin-Kasteleyn representation of the latter, or to bond percolation when $n = 1$. Another natural model in two dimensions is that on the Manhattan lattice (Fig. 2.2) where all the links on a given line point in the same direction, and where weight p is assigned to nodes at which the loops cross and weight $1 - p$ to those at which they turn (Fig. 2.3, right). See Chap. 5 for further discussion of models on these lattices.

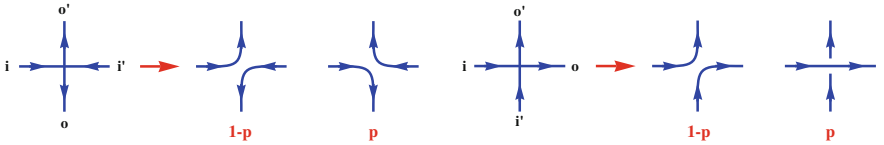

Fig. 2.3 *Left* possible decompositions of a node of the 2D or 3D L lattice (the labelling of links used in Eq. 2.6 is also shown). *Right* decompositions of a node of the 2D Manhattan or 3D K lattice

In this chapter we consider two lattices that allow us to explore the range of critical phenomena possible in three dimensions. These are Cardy's 3D L lattice [4], and a variant, the K lattice (which is similar to the 3D Manhattan lattice of Ref. [4]) that shares the same underlying undirected lattice but has different link orientations. Previous numerical work at $n = 1$ considered a model on the diamond lattice [3]. Much of the discussion will however be independent of the choice of lattice, and even the restriction to four-coordinated nodes can be dropped.

2.2.1 The 3D L and K Lattices

Following Ref. [4], consider two interpenetrating cubic lattices of lattice spacing two, $C_1 = (2\mathbb{Z})^3$ and $C_2 = (2\mathbb{Z} + 1)^3$, displaced from each other by the vector $(1, 1, 1)$. The desired lattice of coordination number four is formed by the intersections of the *faces* of C_1 and C_2—see Fig. 2.4. The 3D L lattice is obtained by orientating the links of this lattice so that each node resembles Fig. 2.3 (left) up to a rotation.

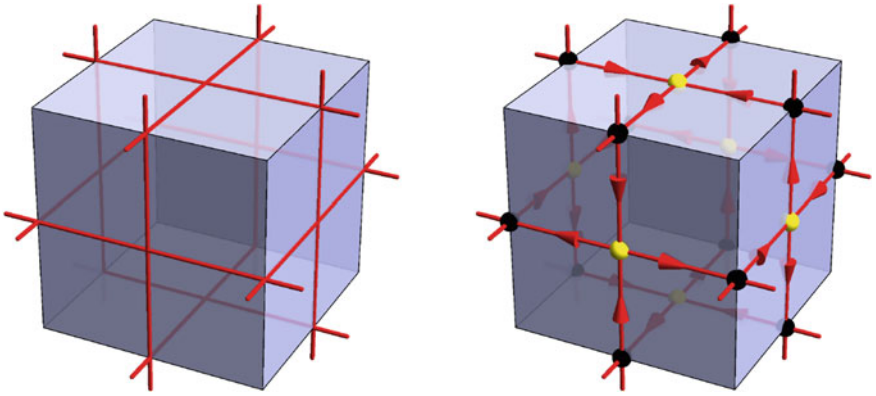

Fig. 2.4 *Left* a cube of C_1, with the lines of intersection with C_2 marked in *red*. These lines form the links of the L and K lattices. *Right* with the orientations corresponding to the L lattice added. The two sublattices of nodes, A and B, are marked in *yellow* and *black* respectively

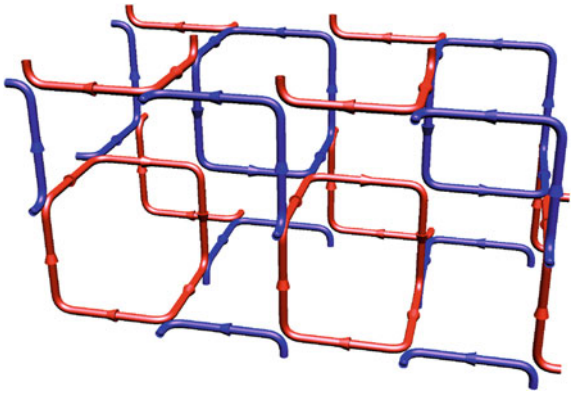

Fig. 2.5 *Left* configuration on the K lattice at $p = 0$

This choice is unique up to reversal of all orientations, and the L lattice has cubic symmetry (some symmetry operations include a reversal of the orientations). For the K lattice, we orient links so that every node resembles Fig. 2.3 (right), and so that nearest-neighbour parallel axes, which are at a distance of $\sqrt{2}$, are oppositely oriented. Again this choice is essentially unique (the eight choices of link orientations are related by reflections), but the resulting oriented lattice is anisotropic.

The K lattice is designed to ensure the existence of both extended and localised phases (phases with and without infinite loops, respectively) for all values of n. The node weights are fixed by Fig. 2.3: the loops reduce to infinite straight lines when $p = 1$, while at $p = 0$ all loops have the minimal length possible on these lattices, which is six. This $p = 0$ configuration is shown in Fig. 2.5. The phase diagram obtained numerically for the K lattice is shown in Fig. 2.6.

While the K lattice only permits a single packing of loops of length six, the L lattice permits four, related to each other by lattice symmetry. The node weights are fixed by picking one of these short-loop configurations to be the configuration which obtains when $p = 1$. Since the exchange $p \to 1 - p$ is equivalent to a lattice symmetry operation, another short-loop configuration obtains at $p = 0$. These configurations provide adequate caricatures of the short loop phases that exist for p close to zero or one (see Fig. 2.6); however an extended phase appears at intermediate p, so long as n is not too large.

The nodes of the L lattice form two sublattices, A and B, as shown in Fig. 2.4. (The sites of A lie at the centres of faces of C_1 and at the centres of edges of C_2, and vice versa for B. The total number of nodes is $3L^3/4$ in an $L \times L \times L$ system.) If we introduce separate node probabilities p_A and p_B, then the four distinct short-loop configurations appear at the four corners of the phase diagram (given by $p_A = \pm 1$, $p_B = \pm 1$). The weight (2.1) corresponds to the line $p_A = p_B = p$.

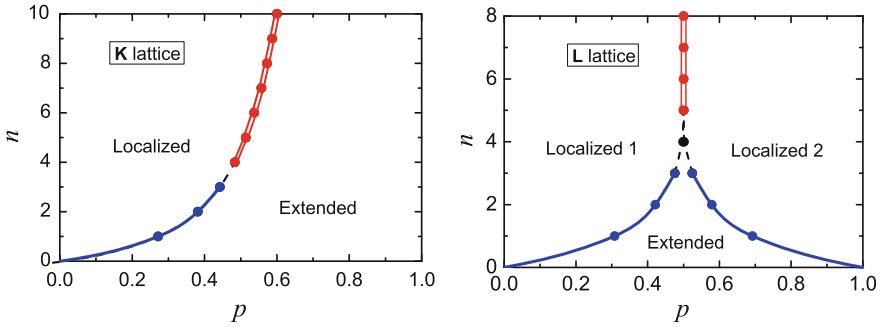

Fig. 2.6 Phase diagrams for the K and L lattices. *Red lines* indicate first order transitions and *blue lines* indicate those that appear to be continuous (*Note* on the L lattice, $p = 1/2$, $n = 4$ lies within the extended phase.)

2.3 Lattice Field Theories

The loop models may be related to lattice 'magnets' for spins located on the links l of the lattice. Neglecting for now complications associated with replicas or supersymmetry (and taking n to be a positive integer), these spins are n-component complex vectors $\mathbf{z}_l$:

$$\mathbf{z}_l = (z_l^1, \ldots, z_l^n), \quad \mathbf{z}_l^\dagger \mathbf{z}_l = n. \tag{2.3}$$

The action for these degrees of freedom will be chosen so that a graphical expansion generates the sum over loop configurations defining Z_{loops}. This leads to a $U(1)$ gauge symmetry,

$$\mathbf{z}_l \sim e^{i\phi_l} \mathbf{z}_l, \tag{2.4}$$

implying that the spins live on CP^{n-1} (defined in Sect. 1.7).

The required action may be written as a sum of contributions from nodes. Letting the trace 'Tr' stand for an integral over the fixed-length vectors $\mathbf{z}$, normalised so Tr $1 = 1$, we write

$$Z = \text{Tr} \exp\Big(- \sum_{\text{nodes}} S_{\text{node}} \Big). \tag{2.5}$$

To define S_{node}, label the links at a node as in Fig. 2.3, with the weight p pairing being $i \to o, i' \to o'$ and the weight $1 - p$ pairing being $i \to o', i' \to o$. Then

$$\exp(-S_{\text{node}}) = p\, (\mathbf{z}_o^\dagger \mathbf{z}_i)(\mathbf{z}_{o'}^\dagger \mathbf{z}_{i'}) + (1-p)\, (\mathbf{z}_o^\dagger \mathbf{z}_{i'})(\mathbf{z}_{o'}^\dagger \mathbf{z}_i). \tag{2.6}$$

The total action is invariant under the gauge transformation (2.4)—the phase ϕ_l cancels between the terms for the two nodes adjacent to link l.

The two terms in $e^{-S_{\text{node}}}$ are in correspondence with the two possible configurations of the node in the loop model. This leads to a simple expression for the partition function in terms of loop configurations $\mathcal{C}$, obtained by writing the Boltzmann weight as a product over nodes and then expanding out this product. Denoting the links lying on a given loop by $1, \ldots, \ell$,

$$\text{Tr} \prod_{\text{nodes}} \exp\left(-S_{\text{node}}\right) = \sum_{\mathcal{C}} W_{\mathcal{C}} \prod_{\text{loops in } \mathcal{C}} \text{Tr}\ (\mathbf{z}_1^\dagger \mathbf{z}_2) \ldots (\mathbf{z}_\ell^\dagger \mathbf{z}_1). \tag{2.7}$$

The integrals over the $\mathbf{z}$s are performed using $\text{Tr}\ z_l^\alpha \bar{z}_l^\beta = \delta^{\alpha\beta}$, leading to a single free colour index for each loop as in Eq. 1.6:

$$Z = \sum_{\mathcal{C}} \sum_{\substack{\text{loop} \\ \text{colours}}} W_{\mathcal{C}} = Z_{\text{loops}}. \tag{2.8}$$

This establishes the desired correspondence between the loop models and models with local 'magnetic' degrees of freedom. We now make the simplest conjectures for the models' continuum descriptions, taking account of the $SU(n)$ global and $U(1)$ gauge symmetries of (2.5).

Note that the lattice action in Eq. 2.5 is not necessarily real. This is not an obstacle to taking the continuum limit (recall for example that complex lattice actions are the norm in quantum problems). In fact it can be an important feature of loop models of this type, leading to imaginary terms in the continuum Lagrangian that are associated with spin configurations of nontrivial topology. These subtleties will not play a role in this chapter, but it will be necessary to consider them more carefully in the next.

2.4 Continuum Descriptions

Let us exchange the vector $\mathbf{z}$, which is a redundant parametrisation of CP^{n-1}, for the gauge-invariant matrix $Q^{\alpha\beta} = z^\alpha \bar{z}^\beta - \delta^{\alpha\beta}$. In addition to being Hermitian and traceless, Q obeys the nonlinear constraint

$$(Q+1)^2 = n\,(Q+1). \tag{2.9}$$

In the continuum we may either retain this constraint, giving the CP^{n-1} sigma model,

$$\mathcal{L}_\sigma = \frac{1}{2g}\,\text{tr}\ (\nabla Q)^2 \qquad (\&\ \text{constraint on } Q) \tag{2.10}$$

or we may use a soft-spin formulation in which Q is an arbitrary traceless Hermitian matrix:

$$\mathcal{L}_{\text{soft}} = \text{tr } (\nabla Q)^2 + t \text{ tr } Q^2 + g \text{ tr } Q^3 + \lambda \text{ tr } Q^4 + \lambda' (\text{tr } Q^2)^2. \tag{2.11}$$

We will see shortly that the extended phase of the loop models corresponds to the ordered phase of the CP^{n-1} model, with $\langle Q \rangle \neq 0$, and short-loop phases correspond to disordered phases.

In using the language of the sigma model, we should bear in mind that in three dimensions the field $Q(x)$ can have pointlike topological defects (hedgehogs) associated with the second homotopy group of CP^{n-1}:

$$\pi_2(CP^{n-1}) = \mathbb{Z}. \tag{2.12}$$

These play an important role in the vicinity of the critical point [6–8], and they proliferate in disordered phase; they are of course irrelevant in the ordered phase. In order to accomodate them, the sigma model constraint must be relaxed in the defect core, and the regularisation-dependent physics in the core then determines a finite fugacity for defects. The condensed formulation of Eq. 2.10, with only the single parameter g, is therefore slightly misleading.

The manifold CP^1 is simply the sphere, so at the special value $n = 2$ the above field theories reduce to the sigma model and soft spin incarnations of the $O(3)$ model. At this value of n, the cubic term in $\mathcal{L}_{\text{soft}}$ vanishes, and there is only one quartic term (the latter also holds at $n = 3$). The $O(3)$ spin S is related to Q via the Pauli matrices, $Q = \frac{1}{\sqrt{2}} \sigma^i S^i$, giving

$$\mathcal{L}_{\text{soft}} = (\nabla S)^2 + t\, S^2 + u\, (S^2)^2 \tag{2.13}$$

with $u = \lambda' + \lambda/2$.

This description leads us to expect continuous transitions in the $O(3)$ universality class for the $n = 2$ models. Continuous transitions are also expected for $n < 2$. For $n > 2$, the naive expectation is a first order transition, as a result of the cubic term in $\mathcal{L}_{\text{soft}}$. However we will argue in Sect. 2.8.2 that fluctuations can invalidate this mean field prediction when the spatial dimension is less than four—numerical work is thus required to determine what happens in 3D.

2.5 Correlation Functions

The natural correlation functions in the loop models are the probabilities of various geometrically-defined events. The basic ones are the l-leg 'watermelon' correlators $G_l(x, y)$, defined as the probability that l distinct strands of loop connect x with y (here we use a continuum notation). If all loops close, the number l must of course be even. On the lattice, G_2 can be taken to be the probability that two links lie on the same loop, and G_4 the probability that two nodes are connected by four strands.

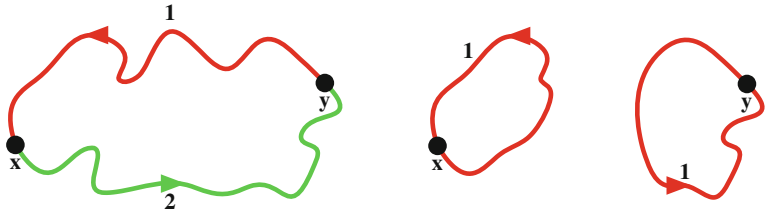

Fig. 2.7 *Left* $Q^{12}(x)$ is a two-leg operator, absorbing an incoming strand of colour 1 and emitting an outgoing one of colour 2. This allows us to form $G_2(x, y)$. *Right* with only a single colour at our disposal (when $n = 1$) we cannot control the topology of the strands passing through x and y

These geometrical observables may be expressed as correlation functions of Q. At a formal level, the relationships follow straightforwardly from the graphical expansion of Sect. 2.3, but they may also be easily guessed by thinking of the loops as worldlines of **z** quanta, i.e. by viewing one of the spatial directions as the imaginary time direction for a quantum problem (as in Sect. 1.3.2). These worldlines come in n colours, one for each component of **z**, and since z^α is a complex field they carry an orientation distinguishing particles from antiparticles.

In particular, the operator $Q_l^{\mu\nu} = z_l^\mu \bar{z}_l^\nu$ with $\mu \neq \nu$ absorbs an incoming strand (worldline) of colour μ and emits an outgoing one of colour ν (Fig. 2.7). More precisely, the effect of this operator on the graphical expansion is to force the loop passing through link l to change colour from μ to ν there. This follows from the fact that for link l, the integral appearing in Eq. 2.7 is modified by the presence of the operator from $\mathrm{Tr}\, z_l^\alpha \bar{z}_l^{\alpha'} = \delta^{\alpha\alpha'}$ to $\mathrm{Tr}\, z_l^\alpha \bar{z}_l^{\alpha'} Q_l^{\mu\nu} = A\, \delta^{\alpha\nu}\delta^{\alpha'\mu}$ (for $\mu \neq \nu$), with $A = n/(n+1)$.

Assume that all loops close, i.e. that there are no open strands escaping to infinity or ending on the boundary (we will relax this in Sect. 2.7). Then the correlator $\langle Q_l^{12} Q_{l'}^{21} \rangle$ receives contributions only from configurations in which l and l' are joined (by a loop with one arm of colour 1 and one arm of colour 2, as in Fig. 2.7), and is proportional to the 2-leg correlator:

$$G_2(l, l') = \frac{n}{A^2} \langle Q_l^{12} Q_{l'}^{21} \rangle. \tag{2.14}$$

The factor of n compensates for the fact that there is no sum over colour indices for the loop passing through l and l'. For convenience, we use here the off-diagonal elements of Q to write geometrical correlators, but all Q correlators can be expressed in terms of loops; for example $\langle \mathrm{tr}\ Q_l Q_{l'} \rangle = (n-1) A\, G_2(l, l')$. We may think of the diagonal components of Q as operators which measure the colour of a link.

In the continuum, the higher watermelon correlators may be written[1]:

$$G_{2k}(x, y) \propto \left\langle [Q^{12}(x)]^k [Q^{21}(y)]^k \right\rangle. \tag{2.16}$$

The correlators considered so far involve only two distinct spin indices, so can be written down as long as $n \geq 2$. More complex correlation functions may require the use of more indices. For example, in Sect. 2.9 we will require the probability that a single loop passes through all the links $l_1, \ldots, l_m$, in that order; this can be written down only if $n \geq m$:

$$G(l_1, \ldots, l_m) = \frac{n}{A^m} \left\langle Q^{12}_{l_1} Q^{23}_{l_2} \ldots Q^{m1}_{l_m} \right\rangle. \tag{2.17}$$

2.6 Replicas and Supersymmetry

These formulas highlight a potential problem: the complexity of the geometrical correlation functions we can represent is limited by the number n of spin components at our disposal, which in turn is set by the loop fugacity. The problem is particularly acute at $n = 1$, when we cannot represent any correlation functions at all—indeed the manifold CP^{n-1} degenerates to a point when $n = 1$, and the matrix Q is identically zero.

As mentioned in Sect. 1.3.1, we can resolve this problem either using replica-like limits—for example, we can write the 2-leg correlator in the $n = 1$ loop model as $G_2(x, y) \propto \lim_{n\to 1} \langle Q^{12}(x) Q^{21}(y) \rangle$—or using SUSY. For most of our purposes these formulations are interchangeable, and it is easy to translate between them. We will mostly use the language of replicas, for presentational simplicity and because it allows us to consider noninteger loop fugacities, which will occasionally be useful. The SUSY formulation is useful for certain tasks; it is also reassuring to know that there is a more rigorous formulation of the field theories which avoids ad hoc analytical continuations.

In the SUSY approach, we augment the lattice field theory with additional Grassman degrees of freedom [9–12]. Every occurence of a $\mathbf{z}$ in (2.5) is replaced by a supervector $\boldsymbol{\psi}$ with $n + k$ commuting and k anticommuting components:

$$\boldsymbol{\psi} = (z^1, \ldots, z^{n+k}, \chi^1, \ldots, \chi^k). \tag{2.18}$$

[1] It is sometimes useful to gather operators into irreducible representations of $SU(n)$. The 4-leg operators form a representation of dimension $n^2(n-1)(n+3)/4$, given (in the sigma model) by the tensor (symmetric in α, α' and in β, β')

$$X^{\alpha\alpha'\beta\beta'} = z^\alpha z^{\alpha'} \bar{z}^\beta \bar{z}^{\beta'} - \frac{\delta^{\alpha\beta} z^{\alpha'} \bar{z}^{\beta'} + 3 \text{ other terms}}{n+2} + \frac{\delta^{\alpha\beta}\delta^{\alpha'\beta'} + \delta^{\alpha\beta'}\delta^{\alpha'\beta}}{(n+1)(n+2)} \tag{2.15}$$

The vector $\boldsymbol{\psi}^\dagger$ involves independent Grassman variables $\bar{\chi}$. Again, we enforce $\boldsymbol{\psi}^\dagger\boldsymbol{\psi} = n$; concretely, we may take this to mean that the integral over $\boldsymbol{\psi}$ defining the trace Tr is proportional to $\int \mathrm{d}\boldsymbol{\psi}\mathrm{d}\boldsymbol{\psi}^* \delta\left(\boldsymbol{\psi}^\dagger\boldsymbol{\psi} - n\right)$, where the delta function is defined by expanding in the Grassman variables. See Ref. [13, 14] for reviews of Grassman integration.

In the expansion of the Boltzmann weight in terms of loop configurations (Eq. 2.7), the integrals for a single loop in the graphical expansion become:

$$\mathrm{Tr}\ (\boldsymbol{\psi}_1^\dagger\boldsymbol{\psi}_2)\ldots(\boldsymbol{\psi}_\ell^\dagger\boldsymbol{\psi}_1) = \mathrm{Tr}\ \bar{\psi}_1^{\alpha_1}(\psi_2^{\alpha_1}\bar{\psi}_2^{\alpha_2})\ldots(\psi_\ell^{\alpha_{l-1}}\bar{\psi}_\ell^{\alpha_\ell})\psi_1^{\alpha_\ell}. \tag{2.19}$$

As before, the formula Tr $\psi_l^\alpha\bar{\psi}_l^\beta = \delta^{\alpha\beta}$ forces all the spin indices to be equal, say to α. However a reordering of the ψs is required before using this formula, and this gives a minus sign if ψ^α is fermionic. This leads to a cancellation between bosonic and fermionic colours, so that the sum over α gives the desired loop fugacity, $(n+k)-k = n$, irrespective of k.

While the partition function and its loop expansion are independent of k, increasing k gives access to more operators. Geometrical correlators may be constructed as in the previous section (if we use only bosonic components the formulas are unchanged).

The field $Q_l = \boldsymbol{\psi}_l\boldsymbol{\psi}_l^\dagger - 1$ is now a supermatrix with both bosonic and fermionic blocks, and lives on complex projective superspace, denoted $\mathrm{CP}^{n+k-1|k}$. Correspondingly the SUSY version of $\mathcal{L}_\sigma$ is termed the $\mathrm{CP}^{n+k-1|k}$ sigma model. We will return to this field theory briefly in Chap. 3. Both the lattice Boltzmann weight and $\mathcal{L}_\sigma$ are invariant under 'rotations' of $\boldsymbol{\psi}$ which preserve $\boldsymbol{\psi}^\dagger\boldsymbol{\psi}$ (superunitary tranformations).

2.7 Phases of the CP^{n-1} Model and Loops

When the CP^{n-1} spins are disordered, correlators such as G_2 decay exponentially ($G_2(r) \sim r^{-1}e^{-r/\xi}$), indicating that long loops are exponentially suppressed. This corresponds to the short-loop phase. On approaching a critical point, the correlation length ξ—a measure of the typical linear size of a loop—diverges as $\xi \sim |p - p_c|^{-\nu}$.

Precisely at criticality, the anomalous dimension η of the field Q determines the decay of $G_2(x, y)$,

$$G_2(x, y) \sim |x - y|^{-(1+\eta)}, \tag{2.20}$$

as well as the fractal dimension of a loop (via a simple scaling relation [15, 16])

$$d_f = \frac{5-\eta}{2}, \tag{2.21}$$

and the probability $P_{\text{link}}(\ell)$ that the loop passing through a given link is of length ℓ:

$$P_{\text{link}}(\ell) \sim \ell^{1-\tau}, \qquad \tau = \frac{11-\eta}{5-\eta}. \tag{2.22}$$

For the critical points discussed in this chapter, η is close to the mean field value $\eta = 0$, so the loops have a fractal dimension close to $5/2$. They are thus more compact than Brownian paths. (Unlike, say, a self-avoiding walk, or the loops which appear in the high temperature expansion of the critical Ising model, which both have fractal dimensions less than two.)

When the spins are ordered, $G_2(x, y)$ becomes long-ranged, indicating the appearance of 'infinite' loops. This is the extended phase. A basic consequence of the CP^{n-1} description is that individual loops are Brownian in this phase, having for example a fractal dimension equal to two. However not all universal properties can be understood by thinking about simple random walks, as we will see in Sect. 2.9.

In the limit of large system size L, there is a sharp distinction between 'finite' and 'infinite' loops, but the nature of the latter depends on whether curves are allowed to terminate at the boundary or whether only closed loops are allowed (as in a system with reflecting or periodic boundary conditions). In the former case the 'infinite' strands end on the boundary, and have length of order L^2 as a result of the fractal dimension being two. When all loops are closed, the 'infinite' loops instead have a length of order L^3: although the fractal dimension of a segment of radius $\lesssim L$ is still two, the number of times a given 'infinite' loop crosses the system is of order L. In this case their joint length distribution shows an interesting universal structure. We will describe this in Sect. 2.9—here we briefly discuss the definition of k-leg correlation functions in the extended phase.

Consider the case where strands can end on the boundary. Microscopically, we have dangling links on the boundary: in the lattice field theory (2.5) we set the spins on these links equal to a fixed vector $\mathbf{z} = \mathbf{e}$ ($\mathbf{e}$ is taken to be real). The graphical expansion then goes through as before, except that a strand of colour α ending on the boundary incurs weight e^{α}. This allows us to separate contributions to correlators associated with finite strands from those associated with infinite strands, i.e. those which end on the boundary.

The boundary condition $\mathbf{z} = \mathbf{e}$ fixes the direction of symmetry breaking in the CP^{n-1} model: we have $\langle Q(x) \rangle = Q_0 \left(\mathbf{e}\mathbf{e}^{\dagger} - 1 \right)$, where Q_0 determines the strength of long range order. Firstly, set $\mathbf{e} = (1, 1, \ldots, 1)$: then the expectation value $\left\langle Q^{12}(x) \right\rangle$ receives contributions only from configurations in which the two strands emanating from x terminate on the boundary (since the two legs have different colour, the loop cannot close in the bulk). Therefore Q_0 is proportional to the probability that a given link lies on an infinite loop. On approaching the critical point, this probability scales with the order parameter exponent β, $Q_0 \sim |p - p_c|^{\beta}$.

Now consider the separation dependence of the l-leg correlation functions. If we define $G_l^{\text{finite}}(x, y)$ to be the probability that x and y are connected by l *finite* strands, l can be either odd or even (unlike at the critical point and in the short loop phase).

Free field theory for the Goldstone modes leads to simple Brownian exponents for these correlators:

$$G_l^{\text{finite}}(x, y) \sim |x - y|^{-l}. \tag{2.23}$$

Each factor of $1/\text{distance}$ can be viewed as the probability that a random walker who starts at one of the points happens to visit the other. It follows from Eq. 2.23 that the curves' fractal dimension is two and the length distribution of finite loops scales as in (2.22) with $\tau = 5/2$.

To see where (2.23) comes from, set $\mathbf{e} = (n, 0, \ldots, 0)$ and write Q in terms of $(n-1)$ complex Goldstone modes $\boldsymbol{\phi}$ (we neglect the massive Higgs mode)

$$Q(x) \propto \hat{\mathbf{z}}\hat{\mathbf{z}}^{\dagger}(x) - 1, \quad \hat{\mathbf{z}}(x) = \left(\sqrt{1 - |\boldsymbol{\phi}(x)|^2},\, \boldsymbol{\phi}(x)\right). \tag{2.24}$$

In writing down a $2k$-leg operator—for example the two-leg operator $Q^{\alpha\beta}$—we can either use colour indices $\alpha > 1$, in which case the corresponding strand is forced to be finite and the correlator involves a Goldstone mode $\phi^{\alpha-1}$, or we can use $\alpha = 1$, in which case configurations in which the strand escapes to infinity dominate, and the leading behaviour of the correlator comes from taking $z^1 \sim 1$. For example $Q^{12} \sim \bar{\phi}^1$, while $Q^{23} \sim \phi^1\bar{\phi}^2$. Since in three dimensions the correlator of two Goldstone modes scales like $1/r$, the corresponding two-point functions are

$$\left\langle Q^{12}(x)Q^{21}(y)\right\rangle \sim |x - y|^{-1}, \quad \left\langle Q^{23}(x)Q^{32}(y)\right\rangle \sim |x - y|^{-2}. \tag{2.25}$$

That on the left is dominated by configurations in which a single infinite strand passes through both x and y, so that they are joined by a single finite strand, while that on the right gives the probability that x and y are joined by a single finite loop, i.e. by two finite strands.

For a system with only closed loops (e.g. with periodic boundary conditions) a similar separation into long and short strands is possible, using an infinitesimal magnetic field to fix the colours of the long strands.

We will discuss the extended phase in more detail in Sect. 2.9. Now we turn to behaviour at the phase transitions.

2.8 Critical Behaviour and First Order Transitions

We begin with a (very brief and incomplete) summary of Monte Carlo results. We then give an analytic picture for the RG flows in the CP^{n-1} model which sheds light on the numerical findings.

2.8.1 Summary of Numerical Results

The following numerical results were obtained by Pablo Serna, Miguel Ortuño, and Andres Somoza. A short account was published in Ref. [17], and a more detailed analysis in Ref. [18]. We take critical exponents for $n = 1$ from earlier work on the diamond lattice [3].

Numerically determined exponents at $n = 2$, which are $\nu = 0.708(5)$, $\gamma = 1.39(1)$ (here $\gamma = (2 - \eta)\nu$), are consistent with known $O(3)$ values [19], confirming the expected universality class of the transition. For $n > 2$, mean field theory predicts a first order transition, as a result of the cubic term in $\mathcal{L}_{\text{soft}}$; simulations suggest that the transition may instead remain continuous at $n = 3$, becoming first order only at larger n. Exponents for $n = 3$ were estimated as $\nu = 0.536(13)$, $\gamma = 0.97(2)$; see Ref. [18] for further details. Recent results for a (2+1)-dimensional bilayer $SU(3)$ magnet, which should be in the same universality class, are also consistent with a continuous transition [20].

For $n = 1$, the transition is continuous (with $\nu = 0.9985(15)$, $d_f = 2.534(9)$) as was first demonstrated for the loop model on the diamond lattice [3]. A continuous transition at $n = 1$ is in agreement with naive expectations: a first-order transition would require that the extended and short-loop phases coexisted at p_c, and that interfaces between them cost a nonzero surface tension; this seems to be ruled out by the independence of the nodes.

A convenient quantity for numerical analysis, which we will require again in Chap. 5, is the 'spanning number'. Consider first of all a system with open boundary conditions for the x direction, so that curves can end on the two faces at $x = 0$ and $x = L$. Then the spanning number n_s is the number of curves which propagate from $x = 0$ to $x = L$. (An equal number propagate in the reverse direction.) This quantity may be related to the free energy with twisted boundary conditions, as we will discuss in detail in Chap. 5, and its mean value $\langle n_s \rangle$ is equal to the spin stiffness in the CP^{n-1} model. In the localisation mapping, which exists for loop fugacity $n = 1$, $\langle n_s \rangle$ is the conductance [1–4].

In the extended phase, $\langle n_s \rangle \sim L$, while $\langle n_s \rangle$ decays exponentially with L in the short loop phase. In the vicinity of a critical point it has the finite-size scaling form

$$\langle n_s \rangle \simeq f\left(L^{1/\nu}(p - p_c)\right). \tag{2.26}$$

If the spanning number is plotted as a function of p, curves for different L are therefore expected to cross at p_c if the transition is continuous.

For computational convenience, we consider systems with periodic boundary conditions, and define n_s by slicing open the system; this is not expected to change the qualitative behaviour described above. Figure 2.8 shows crossings in $\langle n_s \rangle$ for $n = 2$ and $n = 3$ on the K lattice, for system sizes up to $L = 100$. This data leads to estimates for ν, either directly from the slopes of the curves at the crossings or from a scaling collapse using (2.26) plus corrections to scaling. (We present data here only

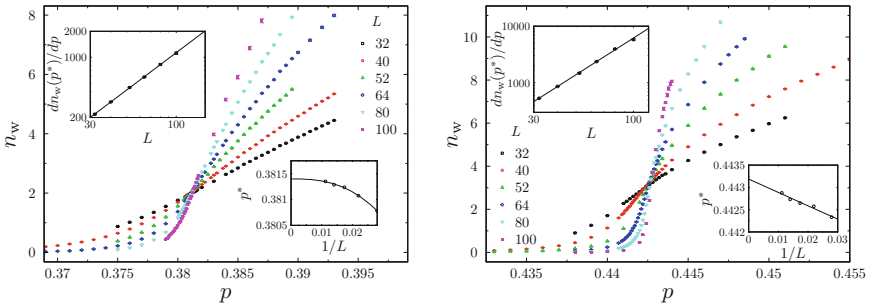

Fig. 2.8 *Left* mean spanning number at $n = 2$. *Main panel* number of spanning curves $n_w(p)$ plotted as a function of p for different system sizes L. *Upper inset* $dn_w(p)/dp$ at crossing points p^* versus L on log-log scales. *Lower inset* p^* versus L. *Right* same for $n = 3$

for the K lattice, but critical behaviour for $n = 1, 2, 3$ is similar on the L and K lattices, and is also consistent with simulations for $n = 1$ on the diamond lattice.)

We are not restricted to considering the mean $\langle n_s \rangle$; for example the probability P_k that n_s is equal to k has a similar finite size scaling form. This leads to the useful result that P_k is a universal, L-independent function of n_s near a critical point. Plotting (say) P_1 against $\langle n_s \rangle$ is thus a test for criticality, as the data should collapse without the need for any fitting parameters. Such plots are shown for $n = 2, 3, 4$ on the K lattice in Fig. 2.9 (left panel).

Data for $n = 2$ and $n = 3$ are compatible with continuous transitions, but stronger deviations from finite size scaling are seen at $n = 3$: we cannot say for certain whether this is a result simply of larger finite size effects, or whether the transition at $n = 3$ is first order, with an extremely large correlation length. Scaling collapse fails at $n = 4$, indicating a weakly first order transition; this is shown even more clearly in the double-peaked form of the probability distribution for N_p (Fig. 2.9, right). On theoretical grounds we expect that the transition at $n = 4$ on the L lattice is also first order, but the situation is complicated by its extreme proximity to $p = 1/2$,

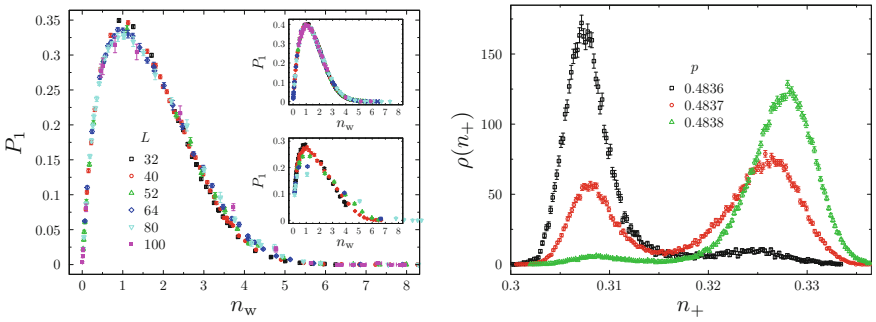

Fig. 2.9 *Left* P_1 plotted against $\langle n_s \rangle$ for $n = 2$ (*upper inset*), $n = 3$ (*main panel*) and $n = 4$ (*lower inset*). *Right* probability distributions for $N_p/(N_p + N_{1-p})$ on the K lattice at $n = 4$

where additional phenomena come into play (Chap. 3). Transitions at larger n are more strongly first order.

The RG picture of the following section implies that there is a universal n_c above which the transition in the CP^{n-1} model becomes first order. We may attempt a very crude estimate of n_c by extrapolating in n to the point at which the latent heat vanishes, using the data for the K lattice at $n \geq 4$. Naive polynomial fits give $n_c \gtrsim 3.3$. However, from the discussion below we expect the latent heat to vanish exponentially, $\sim A \exp(-B/\sqrt{n - n_c})$. Using the data for $n = 4, 5, 6$ to fix these constants gives $n_c = 3.0$. This estimate is not expected to be precise, since the exponential form is valid only asymptotically close to n_c, but it does indicate that n_c is likely to be fairly close to three.

2.8.2 *The* $\mathbf{CP^{n-1}}$ *Model Near* $n = 2$ *and* $d = 4$

At $n = 2$, when the cubic term tr Q^3 in $\mathcal{L}_{\text{soft}}$ vanishes, the upper critical dimension of the CP^{n-1} model is four rather than six.[2] This allows a double expansion in

$$\Delta = n - 2 \qquad \text{and} \qquad \epsilon = 4 - d. \tag{2.27}$$

This idea has been discussed previously for the Q-state Potts model, where the expansion is about the Ising limit [21]. The conclusions below for the CP^{n-1} model are qualitatively identical. In particular, a universal n_c appears, which is greater than the mean field value two when $d < 4$. This helps us to make sense of the numerical results of the previous section.

To begin with, recall the Wilson-Fisher [22] RG equations for the $O(3)$ (or CP^1) Lagrangian (2.13). To lowest nontrivial order these are (after rescaling $u \to u/22$)

$$\frac{\mathrm{d}u}{\mathrm{d}\ln L} = \epsilon u - u^2, \quad \frac{\mathrm{d}t}{\mathrm{d}\ln L} = \left(2 - \frac{5}{11}u\right) t. \tag{2.28}$$

Setting $t = 0$, there are fixed points at $u = 0$ and $u = \epsilon$. For $\epsilon > 0$, the latter is stable in the u direction, and describes the critical CP^1 model, while the former is unstable in the u direction and describes the tricritical point.

We now consider a formal expansion of these equations in Δ (compare the approach to the $2 + \epsilon$ dimensional $O(n)$ model in Ref. [23]), deferring the field-theoretic interpretation until Sect. 2.8.3. The leading contribution is a modification to the RG equation for u:

$$\frac{\mathrm{d}u}{\mathrm{d}\ln L} = -a\Delta + \epsilon u - u^2. \tag{2.29}$$

[2] See however Sect. 2.8.4.

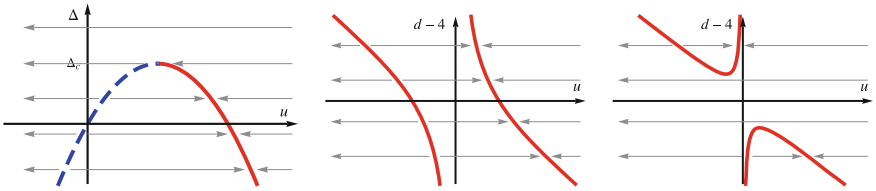

Fig. 2.10 *Left* RG fixed points and flows in the (u, Δ) plane for $d < 4$, showing critical (*red*) and tricritical (*blue, dashed*) fixed points merging at Δ_c. *Centre* RG fixed points and flows in the (u, d) plane for $n < 2$. *Right* the same for $n > 2$

The consistent scaling is to take Δ to be $O(\epsilon^2)$, and u to be $O(\epsilon)$ as at the Wilson Fisher fixed point. Here a is an undetermined universal constant, assumed positive in order to give sensible RG flows.

Figure 2.10 (left) shows the resulting RG fixed points in the (u, Δ) plane for fixed $\epsilon > 0$, i.e. slightly below four dimensions. As Δ is increased, the critical and tricritical fixed points approach each other, annihilating at a critical n_c given to this order by

$$n_c \simeq 2 + \frac{\epsilon^2}{4a}. \tag{2.30}$$

The thermal and leading irrelevant exponents at the critical point are

$$y_t \simeq 2 - \frac{5}{22}\left(\epsilon + \sqrt{\epsilon^2 - 4a\Delta}\right), \quad y_{\text{irr}} \simeq -\sqrt{\epsilon^2 - 4a\Delta}.$$

The anomalous dimension η is $O(\epsilon^2)$, as in the $O(N)$ model. Analogous formulas hold for the Potts model [21].

Precisely at n_c, the irrelevant exponent vanishes and there are logarithmic corrections to scaling. Above n_c, there are no fixed points: the RG flows go off to large negative u, which we interpret as a first order transition.

The strength of this first order transition decreases rapidly as n approaches n_c from above. Integrating Eq. 2.29 from a microscopic scale at which u is positive and of order one to the scale of the correlation length ξ, where u is negative and of order one, gives

$$\xi \sim \exp\left(\frac{2\pi}{\epsilon}\sqrt{\frac{n_c - 2}{n - n_c}}\right). \tag{2.31}$$

Similar forms hold for other quantities such as the latent heat [24]. Note that the asymptotic form $\xi \sim \exp\left(\text{const.}/\sqrt{n - n_c}\right)$ is more general than the lowest-order expansion we are considering here, depending only on the mechanism by which the critical point disappears at n_c [21, 24, 25].

In Fig. 2.10 we show the RG fixed points in the (d, u) plane for $n > 2$ and $n < 2$. Note that when $n < 2$ the fixed points below four dimensions are smoothly connected to those above. This is in agreement with our belief (see Sect. 4.4) that a $6 - \epsilon$ expansion is possible in the model with $n = 1$. For $n > 2$, note the appearance of a branch of fixed points above four dimensions. These fixed points, which are at negative u, are not expected to correspond to genuine critical points, as a result of unboundedness of the fixed point potential (this phenomenon is present even in the $O(N)$ model [22]).

2.8.3 More Concrete Picture

Let us rewrite the soft spin Lagrangian for the CP^{n-1} model as follows:

$$\mathcal{L}_{\text{soft spin}} = \operatorname{tr}(\nabla Q)^2 + t \operatorname{tr} Q^2 + \frac{u}{22} \operatorname{tr} Q^4 + V(Q). \tag{2.32}$$

We have collected the operators which vanish at $n = 2$ into $V(Q)$. There is one of these at cubic and one at quartic order, but formally we allow for higher terms:

$$V(Q) = g_1 \operatorname{tr} Q^3 + g_2 \left(\operatorname{tr} Q^4 - \frac{1}{2} (\operatorname{tr} Q^2)^2 \right) + \cdots \tag{2.33}$$

The two operators shown above vanish when $n = 2$, by virtue of the tracelessness of Q (the second also vanishes at $n = 3$).

The RG equations for t and u must of course be independent of the g_i when $n = 2$, so any term which depends on the latter must have a coefficient proportional to Δ. A similar phenomenon also occurs in the Potts model [21]. To the order that we require, the RG equations for u and g_i are:

$$\frac{\mathrm{d}u}{\mathrm{d}\ln L} = \epsilon u - u^2 - \Delta f(g_1, g_2, \ldots), \quad \frac{\mathrm{d}g_i}{\mathrm{d}\ln L} = \beta_i(g_1, g_2, \ldots). \tag{2.34}$$

(We have checked explicitly that the f term is of order Δ rather than higher order in Δ.) The cubic coupling g_1 is strongly relevant at the four-dimensional Gaussian fixed point, which obstructs a perturbative calculation of f and β_i. However to obtain Eq. 2.29 we need only assume that the g_i flow to fixed point values g_i^* under the RG equations (2.34), and expand around these with $g_i = g_i^* + \delta g_i$:

$$\frac{\mathrm{d}u}{\mathrm{d}\ln L} \simeq \epsilon u - u^2 - \Delta f(g_1^*, g_2^*, \ldots), \quad \frac{\mathrm{d}\delta g_i}{\mathrm{d}\ln L} \simeq -b_{ij} \delta g_j. \tag{2.35}$$

The first of these equations yields Eq. 2.29, with $a = f(g_1^*, g_2^*, \ldots)$. The second yields subleading (order one) irrelevant exponents associated with the operators in $V(Q)$.

2.8.4 Nonuniqueness of the Upper Critical Dimension at $n = 2$

In order to analytically continue in n it is important to realise that it is the operators in $V(Q)$, and not their couplings, which vanish when $n = 2$. We may consider higher-dimensional versions of the loop models discussed here, and this observation leads to the conclusion that for $n = 2$ such models have two distinct upper critical dimensions.

For correlators which can be written down using only two spin indices, we do not need a replica limit (or SUSY). We set $n = 2$ directly, giving the $O(3)$ model with upper critical dimension four. These correlators will thus have Gaussian behaviour at the critical point for $d \geq 4$. However for correlators which require more than two indices, we are forced either to analytically continue in n or to use SUSY. In either case, the cubic term reappears (in the SUSY formulation, i.e. the soft-spin $\mathrm{CP}^{n+k-1|k}$ model, it is str Q^3, where str is the supertrace), leading to a non-Gaussian theory below six dimensions. These correlators are thus expected to have nontrivial behaviour for $d < 6$. This could be tested numerically by a simulation in four dimensions. (An appropriate ensemble of loops could be generated as a byproduct of the simulation of an $SU(2)$ magnet in $3 + 1$ dimensions.)

2.9 Joint Length Distribution in the Extended Phase

In the extended phase, a finite fraction of the links lie on 'long' loops, i.e. those with length of order L^3. How is the total length of these loops divided up between them? This is a natural question not only for the loop models considered here, but also for the worldlines appearing in quantum Monte Carlo and for the loops in a variety of other statistical physics problems (Sect. 2.11).

The answer is given by a one-parameter probability distribution known as the Poisson Dirichlet distribution [26] (here the parameter is n). This distribution appears in many situations which involve an infinite collection of random quantities, $\ell_1, \ell_2, \ldots$, whose sum is fixed. In particular, it has been rigorously proved to apply to the joint distribution of cycle lengths in natural ensembles of random permutations [27–29]—these can be viewed as loop ensembles with no spatial structure. It has been conjectured by Ueltschi and collaborators (with support from simulations) also to apply to loop ensembles with spatial structure, on the basis that when long loops proliferate spatial structure may become unimportant [30–32].

This conjecture for the loop length distribution has not however been related to field theory. Here we show how to derive it using the replica trick. The following derivation extends easily to other loop ensembles in an extended phase and to the random permutation problem.

Label the loops in a configuration $\mathcal{C}$ by $i = 1, \ldots |\mathcal{C}|$, and let ℓ_i denote the length of the ith loop. To begin with, consider the moments $\left\langle \sum_i \ell_i^m \right\rangle$ for integer $m > 1$. We obtain these by integrating the correlation function that gives the probability that m

links lie on the same loop (Eq. 2.17). Switching to a continuum notation, and with a being a nonuniversal operator normalisation constant,

$$\left\langle \sum\nolimits_i \ell_i^m \right\rangle = \frac{n\,(m-1)!}{a^m} \int \mathrm{d}^3 x_1 \ldots \mathrm{d}^3 x_m \left\langle Q^{12}(x_1) \ldots Q^{m1}(x_m) \right\rangle. \tag{2.36}$$

To see this, note that in the graphical expansion of the above m-point function, a given loop configuration gives a nonzero contribution only if all the points x_k lie on the same loop i. For a given configuration and a given loop i, the integrals over x_k then give $\ell_i^m/(m-1)!$, where the factor in the denominator arises because the x_k must appear in a prescribed order around the loop.

In the ordered phase, the dominant contribution to the m-point function in (2.36) comes from the zero mode of $Q(x)$. The setting we are considering here, with only closed loops, corresponds to boundary conditions that preserve global $SU(n)$ symmetry, so we must average over the direction of symmetry breaking. Writing $Q(x) \simeq Q_0\,(\mathbf{z}\mathbf{z}^\dagger - 1)$, this is equivalent to averaging $\mathbf{z}$ over the sphere $\mathbf{z}^\dagger\mathbf{z} = n$. Such averages are given by

$$\mathrm{Tr}\; z^{\alpha_1} \ldots z^{\alpha_q} \bar{z}^{\beta_1} \ldots \bar{z}^{\beta_q} = \frac{n^{q-1} n!}{(n+q-1)!} \left[z^{\alpha_1} \ldots z^{\alpha_q} \bar{z}^{\beta_1} \ldots \bar{z}^{\beta_q} \right]_{\mathrm{G}}, \tag{2.37}$$

where $[\ldots]_{\mathrm{G}}$ is a Gaussian average evaluated using Wick's theorem and $[z^\alpha \bar{z}^\beta]_{\mathrm{G}} = \delta^{\alpha\beta}$. From this we have

$$\left\langle Q^{12}(x_1) \ldots Q^{m1}(x_m) \right\rangle \simeq Q_0^m\, \mathrm{Tr}\, \left(|z^1|^2 \ldots |z^m|^2 \right) = Q_0^m \frac{n^{m-1} n!}{(n+m-1)!}.$$

Combining this with the previous formula and defining $\mathcal{L}_{\mathrm{long}} = Q_0 L^3 n/a$,

$$\left\langle \sum\nolimits_i \ell_i^m \right\rangle = \frac{n!(m-1)!}{(n+m-1)!} \mathcal{L}_{\mathrm{long}}^m. \tag{2.38}$$

Above, m is an integer greater than one (in order for the correlators to make sense). As a result, only long loops[3] contribute to the sum at leading order in L. We expect that we can analytically continue to $m = 1$ if we take the sum to run only over long loops, which we denote by a prime: $\left\langle \sum_i' \ell_i \right\rangle = \mathcal{L}_{\mathrm{long}}$. We see that $\mathcal{L}_{\mathrm{long}}$ is the total length of long loops. This can be confirmed by the arguments of Sect. 2.7 relating the order parameter to the fraction of links on long loops. We can also confirm using (2.41) below that the fraction of links on long loops is non-fluctuating in the thermodynamic limit.

[3] Picking any $u < 3$, only loops longer than L^u contribute at leading order. The fraction of links on long loops is not sensitive to precisely where (on a logarithmic scale) we put the division between long and short loops, since in the thermodynamic limit the total length is split between loops whose length is of order L^3 and those whose length is of order L^0.

In order to fix the full probability distribution we must calculate more general moments,

$$C(m_1, \ldots, m_q) \equiv \mathcal{L}_{\text{long}}^{-\sum_k m_k} \left\langle {\sum}'_{i_1,\ldots,i_q} \ell_{i_1}^{m_1} \ldots \ell_{i_q}^{m_q} \right\rangle, \tag{2.39}$$

but these follow by an immediate extension of the above reasoning. We integrate an $(m_1 + \ldots + m_q)$-point correlation function with arguments

$$x_1^{(1)}, \ldots, x_{m_1}^{(1)} ; \ \ldots \ ; \ x_1^{(q)}, \ldots, x_{m_q}^{(q)}, \tag{2.40}$$

in which the coordinates $x_1^{(k)}, \ldots x_{m_k}^{(k)}$ are forced by a product of two-leg operators to lie on the same loop. A different set of spin indices is used for each k, so $\sum_{k=1}^{q} m_k$ distinct indices are used in total. We find

$$C(m_1, \ldots, m_q) = \frac{n^q \, \Gamma(n) \, \Gamma(m_1) \cdots \Gamma(m_q)}{\Gamma\left(n + m_1 + \cdots + m_q\right)}. \tag{2.41}$$

Take the ℓ_i to be ordered in decreasing size, and define normalised loop lengths by $\zeta_i = \ell_i / \mathcal{L}_{\text{long}}$ (so that $\sum_i' \zeta_i = 1$). The above formula shows that in the limit of large system size the probability distribution for the ζ_i is the Poisson-Dirichlet distribution, denoted PD(θ), with $\theta = n$.

This distribution may be defined as the limit of a Dirichlet distribution for N variables as $N \to \infty$. The Dirichlet distribution is given in terms of θ by

$$P_{\text{Dirichlet}}(\zeta_1, \ldots, \zeta_N) = \frac{\Gamma(\theta)}{\Gamma(\theta/N)^N} \, (\zeta_1 \zeta_2 \ldots \zeta_N)^{\theta/N - 1} \, \delta\Big(\sum\nolimits_i \zeta_i - 1\Big). \tag{2.42}$$

Calculating moments of (2.42) and taking the $N \to \infty$ limit reproduces the above formula for $C(m_1, \ldots, m_q)$.

Note that to obtain the full distribution we had to use an arbitrarily large number of colour indices. Translating the derivation into the SUSY language, this means we must consider the $\text{CP}^{n+k-1|k}$ model for arbitrarily large k.

2.9.1 Length Distribution for a Single Loop

The above formulas allow us to extend our previous formula for the probability distribution $P_{\text{link}}(\ell)$ of the loop through a given link to the regime where ℓ is comparable with the system volume:

$$P_{\text{link}}(\ell) \simeq \begin{cases} c \, \ell^{-3/2} & (1 \ll \ell \ll L^2) \\ \theta \, \mathcal{L}_{\text{tot}}^{-1} \left[1 - \ell / \mathcal{L}_{\text{long}}\right]^{\theta - 1} & (L^2 \ll \ell \leq \mathcal{L}_{\text{long}}). \end{cases} \tag{2.43}$$

Recall that $\theta = n$. Here $\mathcal{L}_{\text{tot}}$ is the total loop length, given in our lattice models by $\mathcal{L}_{\text{tot}} = 3L^3/2$. In addition the above expressions involve two nonuniversal constants: c, and the fraction of links that lie on long loops, $f = \mathcal{L}_{\text{long}}/\mathcal{L}_{\text{tot}}$.

The above formula for the regime $\ell \gg L^2$ is obtained from the marginal distribution for a single ζ coming from Eq. 2.42:

$$P(\ell) = \frac{\ell \lim_{N\to\infty} N\, P_{\text{marg}}(\ell/\mathcal{L}_{\text{long}})}{\mathcal{L}_{\text{tot}} \times \mathcal{L}_{\text{long}}}, \quad P_{\text{marg}}(\zeta) = \Gamma(\theta) \frac{\zeta^{\theta/N-1}(1-\zeta)^{\theta-\theta/N-1}}{\Gamma(\theta/N)\,\Gamma([1-1/N]\theta)}.$$

The factor of ℓ in the first formula arises because a link chosen at random is more likely to lie on a long loop than a short one.

A notable feature of Eq. 2.43 is that $P(\ell)$ is non-monotonic when $\theta < 1$, developing a divergence at $\ell = \mathcal{L}_{\text{long}}$. This is perhaps not surprising, since the limit $n = 0$ describes the universality class of a single 'dense' polymer which fills the entire lattice: for this problem the entire probability distribution concentrates on $l = \mathcal{L}_{\text{tot}}$.

In the models discussed so far, where loops carry an orientation, we must consider $n < 1$ in order to see this divergence. However in the *unoriented* loop models discussed in the next section, the distribution PD(θ) appears with $\theta = n/2$—this follows by simple modifications of the above arguments—so the divergence can be seen at loop fugacity $n = 1$. (See also Sect. 2.11.) Further discussion of the loop length distribution, together with numerical results, may be found in Ref. [33].

2.10 Unoriented Loop Models

The loop models discussed so far are defined on oriented lattices, and the loops carry an orientation. We may define similar loop models on unoriented lattices, for example on the unoriented version of the L/K lattice. We then allow three distinct pairings at each node.

The lattice mapping (2.5) is easily adapted to such cases, leading to a field on real projective space, RP^{n-1}. Field theories similar to $\mathcal{L}_\sigma$ and $\mathcal{L}_{\text{soft}}$ apply, but with real-valued Q.

In three dimensions, the phenomenology—with transitions between short-loop and extended phases—is similar to that of the oriented loop models; preliminary numerical simulations for the case $n = 1$ (the RP^0 model) give $\nu \sim 0.9$ and $d_f \sim 2.54$ [34]. In two dimensions, however, the oriented and unoriented models show very different behaviour, as we will discuss in Chap. 5.

2.11 Loops in Frustrated Systems

In this section we conjecture field theories for 'fully packed' 3D loop models. These are similar to the completely packed models discussed above, but include

an additional element of frustration which changes the continuum descriptions. The simplest example is the fully packed loop model on the cubic lattice. Unoccupied links are allowed, but every node is visited by precisely one loop:

$$Z_{\mathrm{FPL}} = \sum_{\substack{\text{fully-packed} \\ \text{loop configs.}}} n^{\text{no. loops}}. \tag{2.44}$$

The limit $n = 0$ corresponds to a single dense polymer, or Hamiltonian walk, studied numerically in Ref. [35, 36]. (It would be interesting to use the field theory below to analyse these results.)

In analogy to various other constrained three-dimensional systems such as dimer models and spin ice, we expect the full-packing constraint to give rise to an emergent non-compact gauge field in the continuum [37, 38]. Such problems are said to be in a 'Coulomb' phase. We briefly recall the argument for such a field.

Let n_l be the occupation number of the link l, so that $n_l = 1$ if a loop passes through the link and $n_l = 0$ otherwise. Denoting the two sublattices of the cubic lattice by A and B, let $e_{l\mu}$ be the unit vector directed along link l from the site in A to the site in B ($\mu = 1, 2, 3$ is the spatial index). Now define the configuration-dependent vector field

$$B_{l\mu} = \left(n_l - \frac{1}{3}\right) e_{l\mu}. \tag{2.45}$$

The lattice divergence of this field, defined by a sum over the links adjacent to a given site i, vanishes as a result of full packing: $(\nabla_\mu B_\mu)_i = 0$. Assuming that B_μ provides an appropriate language for coarse-graining, and defining $B = \nabla \times A$ to take account of the divergence constraint, the simplest continuum Lagrangian for this field is

$$\mathcal{L}_{\mathrm{Coulomb}} = \frac{\kappa}{2}(\nabla \times A)^2. \tag{2.46}$$

This Lagrangian is only part of the continuum description. For a complete one we must take into account all the conserved fluxes in the lattice model. $\mathcal{L}_{\mathrm{Coulomb}}$ describes one type of conserved flux, which is carried by B. The loops are *not* flux lines for B. They do however carry another conserved flux, which is related to the fact that—after we have realised the loop fugacity via a sum over colours—the colour of a strand is conserved along its length. The interesting feature of this model is that while the two types of flux are made up of the same degrees of freedom microscopically, they decouple in the IR.

In order to see what the symmetries of the problem are, we write a lattice field theory analogous to Eq. 2.5:

$$Z_{\mathrm{FPL}} = \mathrm{Tr} \sum_{\{n_l\}} \delta(\nabla.B) \prod_{\langle ij \rangle} \left(\delta_{n_{ij},0} + \delta_{n_{ij},1} \mathbf{S}_i.\mathbf{S}_j\right). \tag{2.47}$$

The sum is over occupation numbers $n_l = 0, 1$, and the trace denotes the integral over $O(n)$ spins $\mathbf{S}$ living on the sites i (with the constraint $\mathbf{S}_i^2 = n$). A graphical expansion of the $\mathbf{S}$-dependent part of the Boltzmann weight generates the loop fugacity in the same manner as in Sect. 2.3.

In the absence of defects in the full-packing constraint, the Boltzmann weight for the spins in (2.47) has the $\mathbb{Z}_2$ gauge symmetry $\mathbf{S}_i \to \chi_i \mathbf{S}_i$, with $\chi_i = \pm 1$. The local gauge-invariant degree of freedom is therefore really a point on RP^{n-1} rather than on the sphere S^{n-1}. For brevity, we neglect this in the following discussion. This neglect is viable when $\mathbf{S}$ is ordered, i.e. in a phase with extended loops (see Chap. 5 for a more careful discussion of $\mathbb{Z}_2$ gauge symmetries in a 2D context). We expect (2.44) to yield an extended phase if n is smaller than some critical value; extended loops are of course guaranteed as $n \to 0$. We consider here only such a phase.

We also make the assumption that lattice symmetries are not spontaneously broken in the extended phase of (2.44). Such symmetry breaking would certainly be induced by adding sufficiently strong interactions favouring, for example, parallel loop segments. The resulting transitions are expected to correspond to Higgs transitions in which fluctuations of the gauge field become massive [39–42].

With these caveats, we conjecture the following continuum description for the extended phase:

$$\mathcal{L}_{\mathrm{FPL}} = \frac{K}{2}(\nabla \mathbf{S})^2 + \mathcal{L}_{\mathrm{Coulomb}} \qquad (\mathbf{S}^2 = 1). \tag{2.48}$$

We have rescaled the $O(n)$ spin in accordance with convention. The spin is ordered and exhibits Goldstone fluctuations; in this phase, symmetry-allowed interactions between A and $\mathbf{S}$ are irrelevant. Note that while A and $\mathbf{S}$ are independent in the IR, some operators—such as the one-leg operator, which involves a violation of the $\nabla . B$ constraint—combine both sectors. (Note also that at $n = 1$ the Goldstone modes associated with $\mathbf{S}$ vanish, so this field does not contribute to thermodynamic properties of the model; for this value of n it is only required for geometrical correlators.)

The simple idea above can be extended to other loop models. One is a classical loop model which appears in the study of the uniform resonating valence bond wavefunction for a spin-1/2 magnet on the cubic lattice [43]. (This wavefunction is the equal amplitude superposition of singlet coverings of the lattice, as described in Sect. 1.6.) Operator expectation values in this quantum state map to correlators in a classical loop model similar to (2.44), and a lattice partition function similar to 2.47 may be written. The naive continuum limit is again (2.48), with $n = 4$. This is consistent with the simulations of Ref. [43], which show the coexistence of long loops with Coulombic correlations.[4]

A class of two-flavour loop models may be approached in a similar manner. Classical spin ice is one special case of these models [44] and the four-colouring model on the pyrochore lattice is another [45]; in 2D they are well studied and can

[4] The $O(4)$ symmetry in this field theory is at first sight surprising, as it describes a wavefunction for an $SU(2)$ magnet. The symmetry is broken to $SU(2)$ if e.g. the amplitude of a singlet covering depends on the number of parallel singlets.

be understood using height model mappings [46, 47]. They involve configurations of two flavours of loops (call them + and − loops) on a four-coordinated lattice such as the diamond. Allowable configurations are those in which every node is visited by one + and one − loop. The two flavours can be assigned separate fugacities:

$$Z_{+-} = \sum_{\substack{\text{allowed} \\ \text{loop configs.}}} n_+^+ \, n_-^-. \tag{2.49}$$

For these models we need two types of spin, one for each flavour, with n_+ and n_- components respectively. In some cases these models also have alternative descriptions which involve only gauge fields [45]; roughly speaking, the additional gauge fields are dual to the Goldstone modes in the description above.

For some of the models discussed in this section the loop length distribution has been determined numerically. The above descriptions and the arguments of Sect. 2.9 imply that the Poisson-Dirichlet distribution with $\theta = 1/2$ applies to the loops in spin ice studied in Ref. [44], that with $\theta = 1$ applies to those in the four-colouring model [45], and that with $\theta = 2$ applies to those in Ref. [43].

2.12 Conclusion

This chapter has described the relationship of a class of three-dimensional loop models to the CP^{n-1} model, and some simple consequences of this mapping for universal behaviour at phase transitions and in the extended phase. We also tackled some related issues such as the RG fixed point structure for the CP^{n-1} model.

When thinking about field theory in terms of random geometry—e.g. in terms of ensembles of loops—it should be borne in mind that a given critical field theory may be related to more than one universality class of geometrical model. The CP^{n-1} and RP^{n-1} models in particular are related to a remarkable variety of geometrical problems.

A simple example of this non-uniqueness is provided by CP^1. We have seen that this field theory is related to an ensemble of loops with fugacity $n = 2$. However, in its incarnation as the $O(3)$ model, it also has a well-known high temperature expansion that generates an ensemble of loops of fugacity three. These have different universal properties—for example, since the two-leg operator for these loops is no longer Q but instead a bilinear in Q, they have a different fractal dimension.

The difference between these two types of loops is essentially that the first kind are worldlines of $\mathbf{z}$, while the second are worldlines of the composite field Q. We might therefore ask whether worldlines of Q generate natural geometrical ensembles for other values of n. In two dimensions, this leads to an interesting relationship with Potts domain walls—this is described in Appendix A—as well as with branched polymers [48].

A feature of the CP^{n-1} models which we have not so far discussed is their relationship to gauge theories, in which the confinement of $\mathbf{z}$ into the composite field Q is effected by a fluctuating gauge field. This will become important when we discuss line defects in Chap. 4. It is also important for quantum magnets described by CP^{n-1} and related field theories [8]. In the next chapter we consider the connections between the loop models and such magnets.

References

1. I.A. Gruzberg, A.W.W. Ludwig, N. Read, Phys. Rev. Lett. **82**, 4524 (1999)
2. E.J. Beamond, J. Cardy, J.T. Chalker, Phys. Rev. B **65**, 214301 (2002)
3. M. Ortuño, A.M. Somoza, J.T. Chalker, Phys. Rev. Lett. **102**, 070603 (2009)
4. J. Cardy, in *50 Years of Anderson Localization*, ed. by E. Abrahams (World Scientific, Singapore, 2010)
5. A. Nahum, J.T. Chalker, Phys. Rev. E **85**, 031141 (2012)
6. M. Kamal, G. Murthy, Phys. Rev. Lett. **71**, 1911 (1993)
7. O.I. Motrunich, A. Vishwanath, Phys. Rev. B **70**, 075104 (2004)
8. T. Senthil, L. Balents, S. Sachdev, A. Vishwanath, M.P.A. Fisher, Phys. Rev. B **70**, 144407 (2004)
9. A.J. McKane, Phys. Lett. A **76**, 22 (1980)
10. G. Parisi, N. Sourlas, J. Phys. Lett. **41**, L403 (1980)
11. N. Read, H. Saleur, Nucl. Phys. B **613**, 409 (2001)
12. C. Candu, J.L. Jacobsen, N. Read, H. Saleur, J. Phys. A **43**, 142001 (2010)
13. K. Efetov, *Supersymmetry in Disorder and Chaos* (Cambridge University Press, Cambridge, 1997)
14. F. Haake, *Quantum Signatures of Chaos* (Springer, Berlin, 1991)
15. H. Saleur, B. Duplantier, Phys. Rev. Lett. **58**, 2325 (1987)
16. J. Kondev, C.L. Henley, Phys. Rev. Lett. **74**, 4580 (1995)
17. A. Nahum, J.T. Chalker, P. Serna, M. Ortuño, A.M. Somoza, Phys. Rev. Lett. **107**, 110601 (2011)
18. A. Nahum, J.T. Chalker, P. Serna, M. Ortuño, A.M. Somoza, Phys. Rev. B **88**, 134411 (2013)
19. M. Campostrini, M. Hasenbusch, A. Pelissetto, P. Rossi, E. Vicari, Phys. Rev. B **65**, 144520 (2002)
20. R.K. Kaul, Phys. Rev. B **85**, 180411 (2012)
21. K.E. Newman, E.K. Riedel, S. Muto, Phys. Rev. B. **29**, 302 (1984)
22. K.G. Wilson, M.E. Fisher, Phys. Rev. Lett. **28**, 240 (1972)
23. J.L. Cardy, H.W. Hamber, Phys. Rev. Lett. **45**, 499 (1980)
24. J.L. Cardy, M. Nauenberg, D.J. Scalapino, Phys. Rev. B **22**, 2560 (1980)
25. R.J. Baxter, J. Phys. C **6**, L 445 (1973)
26. J.F.C. Kingman, J. Roy. Statist. Soc. B **37**, 1 (1975)
27. O. Schramm, Israel J. Math. **147**, 221 (2005)
28. D. Ueltschi, J. Math. Phys. **54**, 083301 (2013)
29. C. Goldschmidt, D. Ueltschi, P. Windridge, Contemp. Math. **552**, 177 (2011)
30. S. Grosskinsky, A.A. Lovisolo, D. Ueltschi, J. Stat. Phys. **146**, 1105 (2011)
31. D. Ueltschi, J. Math. Phys. **54**, 083301 (2013)
32. C. Goldschmidt, D. Ueltschi, P. Windridge, Contemp. Math. **552**, 177 (2011)
33. A. Nahum, J.T. Chalker, P. Serna, M. Ortuño, A.M. Somoza, Phys. Rev. Lett. **111**, 100601 (2013)
34. P. Serna, M. Ortuño, A.M. Somoza, A. Nahum, J.T. Chalker, Critical Behaviour in 3D Unoriented Loop Models (in preparation)

35. J. Jacobsen, Phys. Rev. Lett. **100**, 118102 (2008)
36. J. Jacobsen, Phys. Rev. E **82**, 051802 (2010)
37. D.A. Huse, W. Krauth, R. Moessner, S.L. Sondhi, Phys. Rev. Lett. **91**, 167004 (2003)
38. C.L. Henley, Annu. Rev. Condens. Matter Phys. **1**, 179 (2010)
39. S. Powell, J.T. Chalker, Phys. Rev. Lett. **101**, 155702 (2008)
40. D. Charrier, F. Alet, P. Pujol, Phys. Rev. Lett. **101**, 167205 (2008)
41. S. Powell, J.T. Chalker, Phys. Rev. B **80**, 134413 (2009)
42. G. Chen, J. Gukelberger, S. Trebst, F. Alet, L. Balents, Phys. Rev. B **80**, 045112 (2009)
43. A. Fabricio Albuquerque, F. Alet, R. Moessner, Phys. Rev. Lett. **109**, 147204 (2012)
44. L.D.C. Jaubert, M. Haque, R. Moessner, Phys. Rev. Lett. **107**, 177202 (2011)
45. V. Khemani, R. Moessner, S.A. Parameswaran, S.L. Sondhi, Phys. Rev. B **86**, 054411 (2012)
46. J.L. Jacobsen, J. Kondev, J. Stat. Phys **96**, 21 (1999)
47. J.L. Jacobsen, J. Kondev, Nucl. Phys. B **532**, 635 (1998)
48. J. Cardy, J. Phys. A: Math. Gen. **34**, L665 (2001)

http://www.springer.com/978-3-319-06406-2

Critical Phenomena in Loop Models

Nahum, A.

2015, XVII, 141 p. 38 illus., 36 illus. in color., Hardcover
ISBN: 978-3-319-06406-2